HEFAT2010
7th International Conference on Heat Transfer, Fluid Mechanics and Thermodynamics
19-21 July 2010
Antalya, Turkey

ANALYSIS OF THE TURBULENT FLOW DYNAMICS OF AN EXTERNAL GEAR PUMP BY TIME RESOLVED PARTICLE IMAGE VELOCIMETRY

Erturk N[1], Vernet A.[1]* and Castilla R[2].
[1]*Author for correspondence
Department of Mechanical Engineering,
University of Rovira I Virgili,
Tarragona, 43007,
Spain,
E-mail: anton.vernet@urv.cat
[2] Department of Fluid Mechanics,
University Polytechnic of Catalunya,
Terrasa, 08222,
Spain

ABSTRACT

Knowledge of the interactions between mechanical elements and the fluid flow provides improvements in enhancement of the performance of gear pumps. Using Time resolved Particle Image Velocimetry (TRPIV) the fluid flow inside an external gear pump is investigated experimentally for different rotational velocity conditions. The flow field contains multiple gear teeth that interact with each other and the fluid surround. These interactions produce major flow and turbulence non-uniformities. In order to understand the turbulent flow dynamics of the flow system, this paper presents data on the instantaneous and phase-locked ensemble averages as well as the turbulent kinetic energy distributions. Comparison of the experimental data with the numerical simulation is carried out for the same model of the gear pump.

INTRODUCTION

External gear pumps are widely used in industry for the fluid movement through the flow systems at high pressure rates. The transfer of the fluid through the external gear pump is maintained by the rotation of the gears. The fluid in the suction chamber is trapped between the teeth of the gears and the body of the pump. As the gears rotate, the fluid is transported to the impulse chamber under pressure.

Recently, there is a demand to increase the pump performance by reducing its size and increasing the rotational velocity [1,2]. With the current design of the suction and impulse chambers of this gear pump, the volumetric efficiency of the pump decreases when the rotational velocity is increased [3,4]. Gear pumps can produce high frequency pressure pulsations that increase the fluctuations of the delivered flow. In order to reduce these fluctuations, improvements in the geometric design of the tooth profile and the body of the pump are needed. Several numerical studies have been done in order to improve the design of gear pumps. A numerical strategy has been developed for the simulation of external gear pumps that can help in the understanding the flow phenomena occurring in the suction and impulse chambers [5]. The flow pulsation that is produced by external gear pumps has been analysed by using different number of teeth on the driving and driven gears from a theoretical point of view [6]. Investigations show that it is not possible to get an external gear pumps with no delivery fluctuation but it can be minimized [7]. These numerical results need experimental validation.

NOMENCLATURE

D	[m]	Gear diameter
f	[fps]	Frequency rate, (frames per second)
k_{2D}	[m^2/s^2]	Turbulent kinetic energy
P	[bar]	Total pressure
Re	[-]	Reynolds number, $\mathrm{Re} = \omega\rho D^2/\mu$
T_g	[s]	Gearing period
x,y	[m]	Cartesian coordinates
u,v	[m/s]	Velocity components with respect to x,y
u',v'	[m/s]	Fluctuation of the velocity components with respect to x,y
$\langle u\rangle,\langle v\rangle$	[m/s]	Fluctuation of the velocity components with respect to x,y
T_I	[s]	Integral time scale
λ_T	[s]	Taylor microscale
ρ	[kg/m^3]	Density
μ	[Pa·s]	Viscosity
t	[s]	Time
ω	[rad/s]	Rotational velocity

In this paper, the fluid flow in the suction chamber of an external gear pump has been experimentally analyzed by using TRPIV technique. The results of the mean and instantaneous

velocity fields can help to identify internal fluid flow system in order to improve the performance and the design of the pump [8]. The instantaneous 2D velocity measurements have been obtained by PIV. In the last decades, PIV technique has been applied to the studies of a large number of flow problems [9] and flow in turbomachines [10,11]. In this study, TRPIV technique has been used to obtain the velocity time-series from the particle images [12]. By applying this technique, the information about time evolution of the large scale flow structures and the mean velocity fields inside the suction chamber have been obtained. To analyze the turbulent behaviour of the flow in the suction chamber, the velocity time history has been used to obtain random unsteady velocity fluctuations as well as the two dimensional turbulent kinetic energy. Besides, the experimental accuracy of the instantaneous flow field measurements has been carried out according to a validation algorithm [13].

EXPERIMENTAL SETUP AND PROCEDURE

The external gear test pump has two identical cogwheels with eleven teeth for each one. The diameter of the gear is 53.6 mm and the depth is 36 mm. A commercial oil with a density of $\rho = 885$ kg/m^3 and $\mu = 0.028$ Pa·s has been used as fluid in the experiments. The main body of the test pump is completely made by transparent methacrylate as shown in Figure 1. The intake side of the suction chamber is located in horizontal plane of symmetry of the pump. The suction and impulse chambers have a size of 31.8 × 16.8 mm^2.

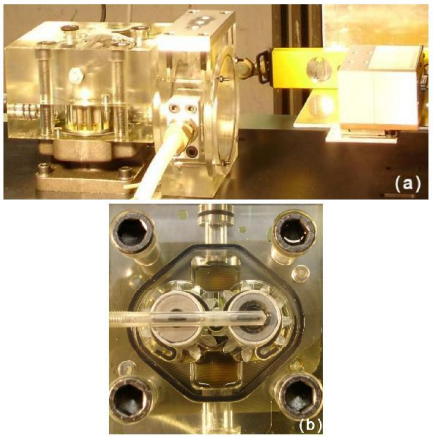

Figure 1 External gear test pump: **a** lateral view; **b** top view.

The test pump is installed in a test bench that is connected by two hydraulic circuits as illustrated in Figure 2. The primary circuit contains the test pump that intakes the fluid from an oil tank and impulses it through a pressure fall of 5-15 bars to the tank again. The secondary circuit contains an olehydraulic motor that supplies power to the test pump and controls its rotational velocity. However it has an inconvenience of having small precision in the selection of the velocity. Therefore, the exact rotational velocity is obtained from the acquired images.

PIV requires flow seeding particles to visualize the flow. In this study, air microbubbles with a diameter of 0.1 mm have been used as particles. These particles have been continuously introduced to the test pump with the help of two air pipes. Porous materials have been placed at the end of the air pipes in order to control the size of the air bubbles.

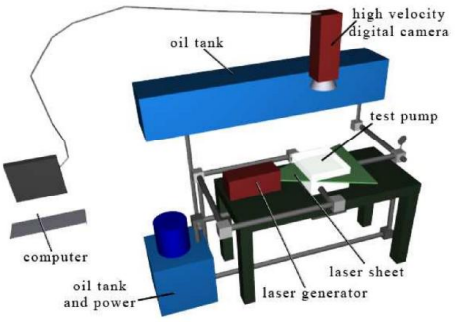

Figure 2 Schematic drawings of the experimental setup.

The particle images are obtained by a Photron Ultima APX-RS camera that can work at 3000 fps for a maximum resolution of 1024×1024 pixels. In these conditions, 2048 images can be recorded from the camera. The sampling rate and the number of recorded frames can be increased by reducing the resolution. A pulsed infrared diode laser from MONOCROM which has a wavelength of 800 nm has been used as illumination source. It allows variable pulse duration ranging from 10 to 100 μs and pulse energy of 2.5 to 25 mJ respectively, with a maximum working frequency of 5 kHz. The laser generates an output light sheet with a thickness of 0.7 mm and wide enough to illuminate the whole suction chamber.

Two series of experiments at different rotational velocities have been carried out by using the configurations of laser and camera together. First experiment is done with a rotational velocity of 28.6 rad/s at 3000 fps using the maximum resolution of the camera and the second one with a rotational velocity of 47.4 rad/s at 4500 fps with a reduced resolution (896 × 784 pixels). Both experiments measure the flow in a region of about 35 × 35 mm that includes the suction chamber and the part of the gears. For each experimental case, the sampling rate is uniform and the laser pulse duration is set to 20 μs. This time interval provides sufficient energy to illuminate the particles and is short enough to avoid image smearing. Considering the rotational velocities of the gear pump, the particle displacement could reach a maximum value of 0.9 pixels and 1.3 pixels respectively for the experimental cases. This error value is larger near gearing area since the velocity is higher in these locations. In the rest of the suction chamber, the mean velocity is smaller than 1 m/s which represent the particle displacements smaller than 0.6 pixels during the laser pulse. Table 1 shows the details for the two experimental cases that have been carried out in this study.

Table 1 Experimental parameters

	Case 1	Case 2
f (fps)	3000	4500
Resolution (pixels)	1024 × 1024	896 × 784
Spatial resolution (pixels)	0.9	1.3
Number of Images	2048	3009
Total time recorded (s)	0.68	0.67
Revolutions recorded	3.2	5.1
P (bar)	15	10
ω (rad/s)	28.6	47.4
ωD (m/s)	1.53	2.54
T_g (s)	0.21	0.13
Re	2595	4304
λ_T (time steps)	7.0	8.2
T_I (time steps)	9.0	9.1

PROCESSING THE PARTICLE IMAGES

The main objective of this study is to analyze the large scale structures that exist in the suction chamber of a gear pump and their evolution when the gear rotates. Thus, the temporal evolution of the structures is obtained by using TRPIV with a sufficient temporal resolution to capture the large scales. Time series of PIV images can be considered as 'time-resolved' if the time step between measurements is smaller than Taylor microscale of the flow [14]. Table 1 shows the estimated values of the Taylor micro scale and integral time scale that are computed from the autocorrelation of the velocity signal in point P (see Figure 3). In both cases the time step between consecutive images is smaller than the Taylor microscale and the integral time scale. Therefore, significant correlation exists between the large-scale structures that are presented in consecutive measurements that allow analyzing its temporal evolution.

The velocity field of the flow is obtained from the time series of the particle images which are recorded by the digital camera. This process is done by using domestic PIV software based on an iterative patterns deformation algorithm with regard to the Local Field Correction PIV method [15]. In order to avoid some significant errors due to the iterative algorithms, boundary treatment method [14] has been implemented by applying a weighting function [16]. The details of the analyzing techniques can be found in Erturk et al. (2008) [17].

In the present work, 64 × 64 pixels interrogation area has been used with a 75% overlapping by considering the adequate particles density in each interrogation area. The oversampling process could affect the estimation of the differential quantities since adjacent velocity data are partially computed from the same particle images. For a 50% interrogation area overlap, the velocities can be considered as weakly correlated. The usual cross-correlation PIV processing has been performed by using fast-Fourier transforms. This significantly reduces the time required for the necessary operations to obtain the instantaneous velocity measurements from PIV images [18].

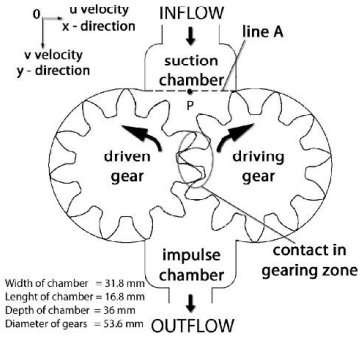

Figure 3 Schematic drawings of the gear pump system.

As a post processing step, a validation algorithm [13] with a modification on the coherence criterion has been applied to the velocity vectors. Basically, the algorithm detects the false vectors, corrects these vectors and calculates the derived flow magnitudes. The process starts by locating a zone where the vector field seems coherent by calculating how many vectors deviates from its neighbours. Then it proceeds scanning through the vector field, visually tracking the local gradient until a location is reached where the vectors clearly deviate from the previously scanned coherent ones. A coherent criterion is defined to decide whether a vector is coherent with its neighbours or not. An adaptive value is used for controlling the coherent criterion. This value is derived from an estimation of the local gradient at each grid point. The local gradient estimation is made for each vector after it is incorporated into current zone. This permits the algorithm to track the local gradient with the changes in the flow and allows larger deviations in the areas of the flow with stronger gradients. An instantaneous velocity field with a region of interest is obtained without using this post processing step as shown in Figure 4a. It can be seen that there are some false vectors that can be identified from the vector map. They are different from the neighbouring ones or outside the physically possible velocity range. Figure 4b shows the result of applying the modified validation algorithm to the same instantaneous velocity vector map. It can be observed that false vectors are correctly validated.

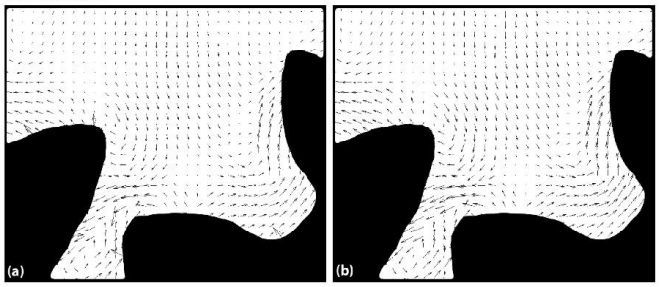

Figure 4 Instantaneous velocity fields for case 2 with: **a** region of interest; **b** the same region of interest after applying the modified validation algorithm.

Conditional Ensemble Averages

The behaviour of the flow structures in the suction chamber can be observed from the velocity time history. The analysis of those velocity fields can be done by observing the flow structures for each single time. This will imply to visualize and study more than 2000 velocity planes. This task can be replaced by the analysis of the typical flow structures that periodically appear in the flow. Computing the autocorrelation of the velocity field can give an idea of existence of periodic structures in the flow. Figure 5 shows the autocorrelation function that is computed from the velocity time history at point P (see Figure 3). It displays a cyclic behaviour which corresponds to the periodical movements of a single tooth at a given position. This indicates that similar flow structures appear in the suction chamber for a fixed location of each tooth. Averaging the velocity fields for a selected tooth location will provide a phase-locked ensemble average that shows the typical flow behaviour for a chosen wheel configuration. Time elapsed between the passages of two consecutive teeth for the same physical location has been used as a proper time scale (gearing period, T_g) due to the strong cyclic character of the flow. The autocorrelation function in Figure 5 corresponds to the passages of three consecutive teeth for the same location. It shows that 58 and 54 particle images for the case 1 and case 2, respectively, have been taken for each gearing period. Thus, 58 and 54 different tooth locations can be observed from the particle images. Only one of these locations has to be chosen in

order to obtain the conditional (phase-locked) ensemble average of the velocity field. The process consists in selecting a single particle image with a defined teeth configuration and a region of interest that includes one gear tooth location. From the correlation function, we can obtain the time events where the teeth are in the same phase. A total of 33 and 53 images are found for averaging of case 1 and case 2, respectively.

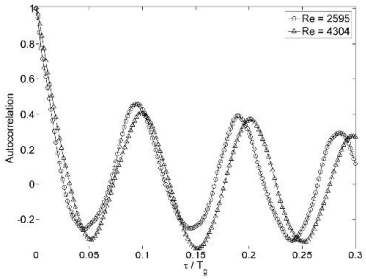

Figure 5 Autocorrelation function in the point P for the experimental case 1 with Re = 2595 and case 2 with Re = 4304.

The turbulence aspects of the flow have been analyzed in the point P (see Figure 3). The energy spectra have been illustrated in Figure 6. Spectra are calculated as the square of the fast Fourier Transform of the velocity fluctuation. Frequencies are normalized with the angular velocity of the experiment. The slope -5/3, corresponding to Kolmogorov's law in homogenous and isotropic turbulence. The two of experimental cases behave in the same way and give acceptable results by reproducing the Kolmogorov energy spectrum.

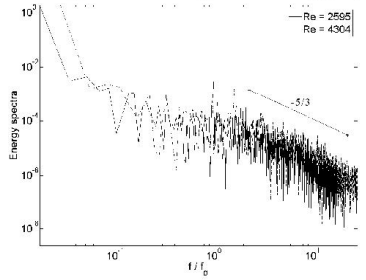

Figure 6 Energy spectra in the point P for the experimental case 1 with Re = 2595 and case 2 with Re = 4304.

RESULTS AND DISCUSSION

The autocorrelation function as illustrated in Figure 5 indicates the strong periodical behaviour of the flow inside the suction chamber. It is inferred that the large-scale structures must be very similar for each single gear tooth passage. This is the basis for using the passages of each gear tooth as a conditional signal to obtain the phase-locked average of the flow. The ensemble average of the velocity field results have been obtained by using three different phases of the gear tooth as shown in Figure 7.

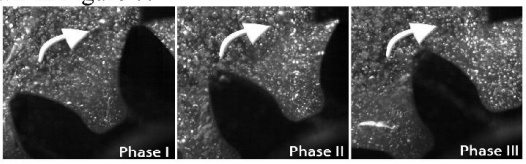

Figure 7 Illustration of the three different phases of the gear tooth profile.

In order to demonstrate the significance of the rotation of the gears into flow, the results have been shown for a region of interest in the suction chamber with the contact in gearing zone. Figure 8 and Figure 9 show the 2D streamlines and magnitude velocity of phase-locked ensemble averages for three different phases. Figure 8 shows the experimental case 1 and Figure 9 shows the experimental case 2. The ensemble average of the velocity field is computed for case 1 and case 2 from 33 and 53 instantaneous vector maps, respectively, for a single selected phase.

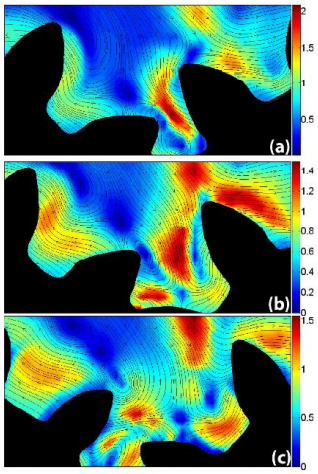

Figure 8 2D streamlines and magnitude velocity of phase locked ensemble averages for case 1: **a** Phase I; **b** Phase II; **c** Phase III.

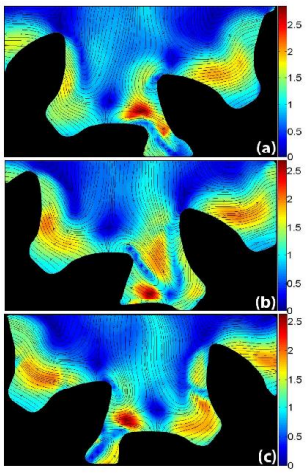

Figure 9 2D streamlines and magnitude velocity of phase locked ensemble averages for case 2: **a** Phase I; **b** Phase II; **c** Phase III.

Two dimensional streamlines are more suitable to visualize the flow structures and to follow their evolution. The three ensembles that are shown in these figures represent the flow structures occurring in the suction chamber close to the gearing zone for a ½ gearing period. A saddle point becomes visible in the figures with Phase I with a focus that is attached to the right-side tooth. These two critical points move and evolve with the gear rotation. Previously, it has been reported that two big foci that dominate the flow in the chamber are present near the walls of the suction chamber and in the upper part of the

suction chamber [17]. These two big foci are present in the suction chamber for all the phases of the gear and the location of the vortex centres is stable during a gear cycle. A focus that that appears in the centre of the gearing zone moves as the gears moves until it joins one of the big focus in the suction chamber. The dynamics of this focus is periodic. It appears when the gearwheel is opening the volume and suctioning the fluid and then moves consecutively to the left-side and to the right-side of the suction chamber. The streamlines results are found to be similar for the experimental cases. The main direction of the flow close to the gearing area of the suction chamber and the location of the foci are almost similar for both cases. The increase in the magnitude of the velocity has been observed close to the gearing zone for both cases. The changes in magnitude can be seen more in the case 1 than case 2. It seems that when the rotational velocity of the gear pump is increased, the flow close to gearing area becomes more stable.

To analyze the turbulent behaviour of the flow close to the gearing zone in the suction chamber, a quantitative measure of the random unsteady velocity fluctuations is obtained from the velocity time history. An ensemble average of the two dimensional turbulent kinetic energy (k_{2D}) can be computed for each phase of gear as:

$$k_{2D} = \frac{1}{2} \cdot \left[\langle u'^2 \rangle + \langle v'^2 \rangle \right] \qquad (1)$$

where u and v are velocity components, the prime denotes the fluctuations and the brackets denote the conditional average.

Contour plots of k_{2D} are illustrated in Figure 10 and Figure 11 for case 1 and case 2, respectively. The figures demonstrate a distribution of turbulent kinetic energy by using the same gear phases. For both experimental cases, the higher levels of the turbulent kinetic energy are found in the backside of the gear tooth and appear in the volume generating in the centre of the gearing zone by gear movement. The smaller values of the turbulent kinetic energy have been found in the upper zones of the gear teeth. The difference between the experimental case 1 and case 2 can be observed in the distribution of the kinetic energy which is sparsely dispersed around the gears for case 1. In the case 2, we do not observe this dispersion of the turbulent kinetic energy.

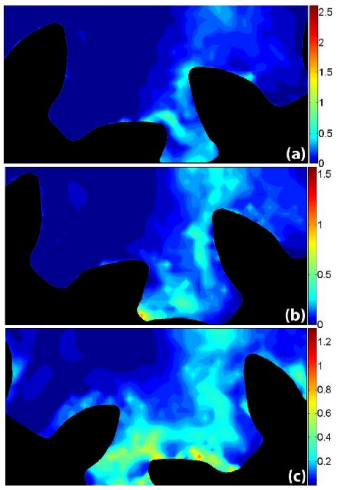

Figure 10 Contour plot of the k_{2D} of turbulent kinetic energy for case 1: **a** Phase I; **b** Phase II; **c** Phase III.

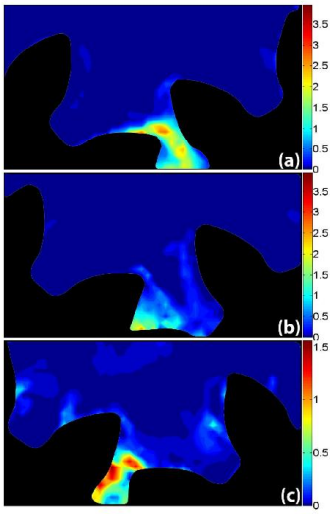

Figure 11 Contour plot of the k_{2D} of turbulent kinetic energy for case 2: **a** Phase I; **b** Phase II; **c** Phase III.

Figure 12 shows the 2D streamlines of the velocity of the flow in the whole suction chamber for experimental case 2 and a numerical study of this flow for a comparison of experimental case 2 at the same phase of the gear. For numerical study, different turbulent models of the flow have been tested for the suction chamber of the same model of the external gear pump. It has been found that the Reynolds Stress Model (RSM) has agreed with the experimental profile near to the gearing zone. The commercial Finite-Volume based code Fluent v.6.3 has been used for the numerical two dimensional simulation. The details of this study can be found in Castilla et al. (2009) [19].

In Figure 12, experimental and numerical results are in qualitative agreement. The locations of the two big vortex centres are similar and they are placed fully integrated into the suction chamber. However, a significant difference is present between the two streamlines fields: a small tip vortex that is formed in the left gear in Figure 12b and this vortex do not appear in the experimental result, Figure 12a. But in the Figure 9c, for a different gear phase (Phase III), we clearly see this small vortex in the left gear. The reason could be probably due to averaging process and the different resolutions that have been used for numerical and experimental studies. Another comparison of experimental and numerical results has been illustrated in Figure 13 as a distribution of turbulent kinetic energy in the whole suction chamber at a fixed position of the gear phase. In both cases, experimental and numerical cases, high levels of turbulence are assembled near gear teeth areas and some levels are in the centre of the suction chamber. However, some significant differences are present between the two distributions of turbulent kinetic energy. In the experimental case, Figure 13a, high levels of turbulent kinetic energy are assembled between two gears and around the gear teeth. But in the numerical case, Figure 13b, the high levels are assembled at the tip points of the gear teeth. At the same time, the increase of kinetic energy is not observed between the two gears. Basically the differences between experimental and numerical results could be attributed the fact that the numerical simulation is done with a larger spatial resolution and in 2D, thus any three dimensional effect is not present.

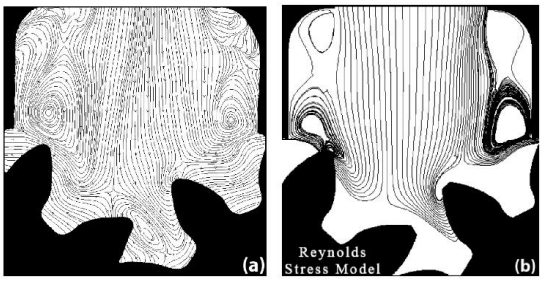

Figure 12 2D streamlines of the suction chamber at a fixed gear phase for case 2: **a** Experimental; **b** Numerical.

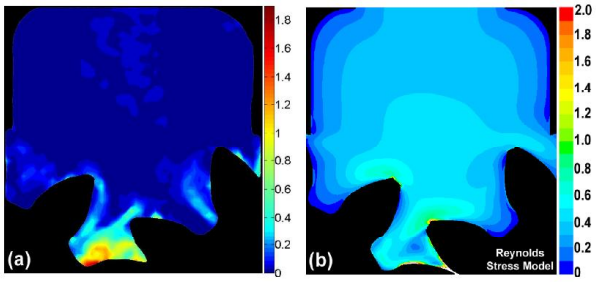

Figure 13 Contour plot of the k_{2D} of turbulent kinetic energy at a fixed gear phase for case 2: **a** Experimental; **b** Numerical.

CONCLUSION

The TRPIV technique has been applied to analyze the behaviour of the flow in the suction chamber and near gearing zone for two different rotational velocities.

The different PIV algorithms and methods have been applied to the TRPIV technique to obtain the velocity field of the flow. The computed autocorrelation of the velocity at one selected location of the suction chamber indicates a periodic behaviour of the flow inside the chamber and this is associated with the gearing period of time. This characteristic is used to obtain phase-locked averages of the flow field. Several gear phases have been used to compute conditional (phase –locked) ensemble average velocity field for each case.

In both experimental cases, smaller critical points as saddles and foci appear in the gearing zone. These critical points move and evolve with the teeth movement. The existence of critical points indicate the three dimensional behaviour of the flow inside the suction chamber.

Comparisons of experimental and numerical 2D streamlines and turbulent kinetic energy data have been illustrated in the whole suction chamber for the same model of the gear pump conditions. Although some similarities have been observed, some significant differences are present between two cases. The reason could be attributed the fact that the numerical simulation is done with a larger spatial resolution and in 2D, thus any three dimensionality effect is not present.

The presented results are done in one plane of the gear pump system. The other planes of the results will be presented in the conference.

Acknowledgements This study was financially supported by projects DPI2009-11204 and DPI2006-14476, the Spanish Ministry of Science and Innovation and FEDER founds.

REFERENCES

[1] Dearn, R., The fine art of gear pump selection and operation, *World pumps*, Vol. 417, 2001, pp. 38-40

[2] Wood, G., External gear pumps for accurate and reliable metering duties, *World pumps*, Vol. 472, 2006, pp. 34-36

[3] Roquet, P., Enhanced design of high pressure gear pumps using environmentally acceptable hydraulic fluids (ECOPUMP), *BRITE-EURAM project*, BE-95-1046, 1998

[4] Castilla, R., Gamez-Montero, P.J., Huguet, D., and Codina, E., Turbulence in internal flows in minihydraulic components, *CIMNE*, 2007, pp. 241-251

[5] Houzeaux, G., and Codina, R., A finite element method for the solution of rotary pumps, *Computers and fluids*, Vol. 36, 2007, pp. 667-679

[6] Manring, N.D., and Kasaragadda, S.B., The theoretical flow ripple of an external gear pump, *Journal of Dynamic Systems Measurements and Control*, Vol. 125, 2003, pp. 396-404

[7] Iyoi, H., and Ishimura, S., χ-Theory in gear geometry, Transaction of ASME Journal of Mechanisms, Transmissions, and Automation in Design, Vol. 105, 1983, pp. 286-290

[8] Castilla, R., Wojciechowski, J., Gamez-Montero, P.J., Vernet, A., and Codina, E., Analysis of the turbulence in the suction chamber of an external gear pump by using Time Resolved Particle Image Velocimetry, Flow Measurements and Instrumentation, Vol. 19, 2008, pp. 377-384

[9] Adrian, R.J., Twenty years of particle image velocimetry, *Experiments in Fluids*, Vol. 39, 2005, pp. 159-169

[10] Wernet, M.P., Development of digital particle image velocimetry for use in turbomachinery, *Experiments in Fluids*, Vol. 28, 2000, pp. 97-115

[11] Wulff, D.L., PIV measurements in pumps, *Design and Analysis of High Speed Pumps*, Vol. 5, 2006, pp. 1-36

[12] Lecordier, B., and Trinité, M., Time Resolved PIV measurements for high speed flows, 3rd International workshop on particle image velocimetry, Santa Barbara, CA, 16-18 September, 1999.

[13] Nogueria, J., Lecuona, A., and Rodriguez, P.A., Data validation, false vectors correction and derived magnitudes calculations on PIV data, *Meas. Sci. Technol.*, Vol. 8, 1997, pp. 1493-1501

[14] Usera, G., Vernet, A., and Ferre, J.A., Consideration and improvements of the analysis algorithms used for Time Resolved PIV of wall bounded flows, 12th international symposium on applications of laser techniques to fluid mechanics, Lisbon, Portugal, 2004.

[15] Nogueria, J., Lecuona, A., and Rodriguez, P.A., Local field correction PIV implemented by means of simple algorithms, and multigrid versions, *Meas. Sci. Technol.*, Vol. 12, 2001, pp. 1911-1921

[16] Lecuona, A., Nogueria, J., and Rodriguez, P.A., Accuracy and time performance of different schemes of the local field correction PIV technique, *Experiments in Fluids*, Vol. 33, 2002, pp. 743-751

[17] Erturk, N., Vernet, A., Ferre, J.A., Castilla, R., and Codina, E., Analysis of the turbulent flow of an external gear pump by time resolved particle image velocimetry, 14th international symposium on applications of laser techniques to fluid mechanics, Lisbon, Portugal, 2008.

[18] Willert, C.E., and Gharib, M., Digital particle image velocimetry, *Experiments in Fluids*, Vol. 10, 1991, pp. 181-193

[19] Castilla, R., Gamez-Montero, P.J., Erturk, N., Vernet, A., Coussirat, M., and Codina, E., Numerical simulation of the turbulent flow in the suction chamber of a gear pump using deforming mesh and mesh replacement, *Flow Measurements and Instrumentation*, Article in Press, 2009